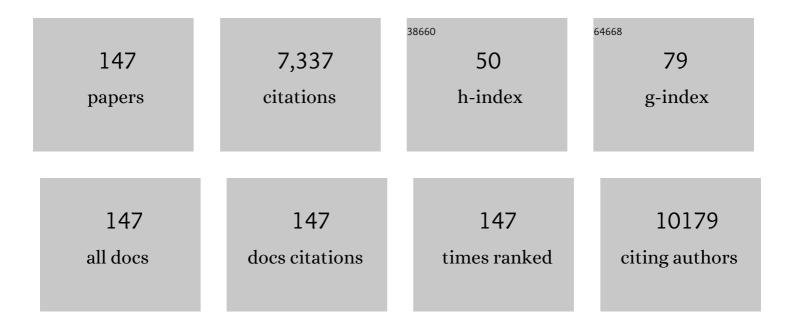
List of Publications by Year in descending order

Source: https://exaly.com/author-pdf/8051988/publications.pdf Version: 2024-02-01



#	Article	IF	CITATIONS
1	POM-based metal-organic framework/reduced graphene oxide nanocomposites with hybrid behavior of battery-supercapacitor for superior lithium storage. Nano Energy, 2017, 34, 205-214.	8.2	308
2	Bimetallic Pt–Au nanocatalysts electrochemically deposited on graphene and their electrocatalytic characteristics towards oxygen reduction and methanol oxidation. Physical Chemistry Chemical Physics, 2011, 13, 4083.	1.3	243
3	Three-Dimensional Interconnected Network of Graphene-Wrapped Porous Silicon Spheres: In Situ Magnesiothermic-Reduction Synthesis and Enhanced Lithium-Storage Capabilities. ACS Applied Materials & Interfaces, 2014, 6, 3546-3552.	4.0	213
4	Effects of structure, composition, and carbon support properties on the electrocatalytic activity of Pt-Ni-graphene nanocatalysts for the methanol oxidation. Applied Catalysis B: Environmental, 2012, 111-112, 208-217.	10.8	211
5	Graphdiyne-Supported Single-Atom-Sized Fe Catalysts for the Oxygen Reduction Reaction: DFT Predictions and Experimental Validations. ACS Catalysis, 2018, 8, 10364-10374.	5.5	202
6	Facile synthesis of nitrogen-doped graphene for measuring the releasing process of hydrogen peroxide from living cells. Journal of Materials Chemistry, 2012, 22, 6402.	6.7	201
7	Aptamer-Guided Silver–Gold Bimetallic Nanostructures with Highly Active Surface-Enhanced Raman Scattering for Specific Detection and Near-Infrared Photothermal Therapy of Human Breast Cancer Cells. Analytical Chemistry, 2012, 84, 7692-7699.	3.2	159
8	Signal Amplification of Graphene Oxide Combining with Restriction Endonuclease for Site-Specific Determination of DNA Methylation and Assay of Methyltransferase Activity. Analytical Chemistry, 2012, 84, 7583-7590.	3.2	142
9	CNTs@SnO ₂ @C Coaxial Nanocables with Highly Reversible Lithium Storage. Journal of Physical Chemistry C, 2010, 114, 22535-22538.	1.5	139
10	Enhancing the electrochemical reduction of hydrogen peroxide based on nitrogen-doped graphene for measurement of its releasing process from living cells. Chemical Communications, 2011, 47, 11327.	2.2	136
11	Graphyne-supported single Fe atom catalysts for CO oxidation. Physical Chemistry Chemical Physics, 2015, 17, 1441-1449.	1.3	136
12	Carbon-coated SnO ₂ nanotubes: template-engaged synthesis and their application in lithium-ion batteries. Nanoscale, 2011, 3, 746-750.	2.8	131
13	Microscopic effects of the bonding configuration of nitrogen-doped graphene on its reactivity toward hydrogen peroxide reduction reaction. Physical Chemistry Chemical Physics, 2013, 15, 6920.	1.3	123
14	Active Site Structures in Nitrogen-Doped Carbon-Supported Cobalt Catalysts for the Oxygen Reduction Reaction. ACS Applied Materials & amp; Interfaces, 2016, 8, 32875-32886.	4.0	120
15	Double-Network Nanostructured Hydrogel-Derived Ultrafine Sn–Fe Alloy in Three-Dimensional Carbon Framework for Enhanced Lithium Storage. Nano Letters, 2018, 18, 3193-3198.	4.5	113
16	Graphyne As a Promising Metal-Free Electrocatalyst for Oxygen Reduction Reactions in Acidic Fuel Cells: A DFT Study. Journal of Physical Chemistry C, 2012, 116, 20472-20479.	1.5	105
17	Nitrogen-Doped Carbon-Wrapped Porous Single-Crystalline CoO Nanocubes for High-Performance Lithium Storage. ACS Applied Materials & Interfaces, 2014, 6, 10602-10607.	4.0	105
18	Self-Templating Synthesis of SnO ₂ –Carbon Hybrid Hollow Spheres for Superior Reversible Lithium Ion Storage. ACS Applied Materials & Interfaces, 2011, 3, 1946-1952.	4.0	104

#	Article	IF	CITATIONS
19	Graphdiyne as a metal-free catalyst for low-temperature CO oxidation. Physical Chemistry Chemical Physics, 2014, 16, 5640-5648.	1.3	102
20	Carbon Nanocapsules as Nanoreactors for Controllable Synthesis of Encapsulated Iron and Iron Oxides: Magnetic Properties and Reversible Lithium Storage. Journal of Physical Chemistry C, 2011, 115, 3612-3620.	1.5	101
21	An electrochemical approach for detection of DNA methylation and assay of the methyltransferase activity. Chemical Communications, 2011, 47, 2844.	2.2	94
22	Electrochemical and Spectroscopic Studies on the Conformational Structure of Hemoglobin Assembled on Gold Nanoparticles. Journal of Physical Chemistry B, 2011, 115, 8627-8637.	1.2	92
23	Low-Potential Detection of Endogenous and Physiological Uric Acid at Uricaseâ	3.2	90
24	Gelâ€Derived Amorphous Bismuth–Nickel Alloy Promotes Electrocatalytic Nitrogen Fixation via Optimizing Nitrogen Adsorption and Activation. Angewandte Chemie - International Edition, 2021, 60, 4275-4281.	7.2	90
25	A graphene–amorphous FePO4 hollow nanosphere hybrid as a cathode material for lithium ion batteries. Chemical Communications, 2012, 48, 2137.	2.2	89
26	Synthesis of Nitrogen-Doped Graphene Quantum Dots at Low Temperature for Electrochemical Sensing Trinitrotoluene. Analytical Chemistry, 2015, 87, 11803-11811.	3.2	89
27	Porous Two-dimensional Iron-Cyano Nanosheets for High-rate Electrochemical Nitrate Reduction. ACS Nano, 2022, 16, 1072-1081.	7.3	89
28	Exploring the Emissive States of Heteroatom-Doped Graphene Quantum Dots. Journal of Physical Chemistry C, 2018, 122, 6483-6492.	1.5	88
29	Chemical Nature of Catalytic Active Sites for the Oxygen Reduction Reaction on Nitrogen-Doped Carbon-Supported Non-Noble Metal Catalysts. Journal of Physical Chemistry C, 2016, 120, 9884-9896.	1.5	87
30	3D Space-Confined Pyrolysis of Double-Network Aerogels Containing In-Fe Cyanogel and Polyaniline: A New Approach to Hierarchically Porous Carbon with Exclusive Fe-N <i> _x </i> Active Sites for Oxygen Reduction Catalysis. Small Methods, 2017, 1, 1700167.	4.6	85
31	Electrolyzing synthesis of boron-doped graphene quantum dots for fluorescence determination of Fe3+ ions in water samples. Talanta, 2017, 164, 100-109.	2.9	83
32	Single-atom-sized Ni–N ₄ sites anchored in three-dimensional hierarchical carbon nanostructures for the oxygen reduction reaction. Journal of Materials Chemistry A, 2020, 8, 15012-15022.	5.2	75
33	Electrochemical measurement of the flux of hydrogen peroxide releasing from RAW 264.7 macrophage cells based on enzyme-attapulgite clay nanohybrids. Biosensors and Bioelectronics, 2011, 26, 4012-4017.	5.3	74
34	Aptamer-Conjugated Au Nanocage/SiO ₂ Core–Shell Bifunctional Nanoprobes with High Stability and Biocompatibility for Cellular SERS Imaging and Near-Infrared Photothermal Therapy. ACS Sensors, 2019, 4, 301-308.	4.0	73
35	Cyanogel-Enabled Homogeneous Sb–Ni–C Ternary Framework Electrodes for Enhanced Sodium Storage. ACS Nano, 2018, 12, 759-767.	7.3	72
36	Real-time fluorescence assay of alkaline phosphatase in living cells using boron-doped graphene quantum dots as fluorophores. Biosensors and Bioelectronics, 2017, 96, 294-299.	5.3	68

#	Article	IF	CITATIONS
37	Hollow porous silicon oxide nanobelts for high-performance lithium storage. Journal of Power Sources, 2015, 274, 951-956.	4.0	67
38	Direct Synthesis of Waterâ€Soluble Aptamerâ€Ag ₂ S Quantum Dots at Ambient Temperature for Specific Imaging and Photothermal Therapy of Cancer. Advanced Healthcare Materials, 2016, 5, 2437-2449.	3.9	67
39	Synthesis of Co2SnO4@C core–shell nanostructures with reversible lithium storage. Journal of Power Sources, 2011, 196, 10234-10239.	4.0	66
40	High specific detection and near-infrared photothermal therapy of lung cancer cells with high SERS active aptamer–silver–gold shell–core nanostructures. Analyst, The, 2013, 138, 6501.	1.7	65
41	Plasmonic Gold Nanohole Array for Surface-Enhanced Raman Scattering Detection of DNA Methylation. ACS Sensors, 2019, 4, 1534-1542.	4.0	65
42	Cyanogelâ€Derived Formation of 3 D Nanoporous SnO ₂ –M _{<i>x</i>} O _{<i>y</i>} (M=Ni, Fe, Co) Hybrid Networks for Highâ€Performance Lithium Storage. ChemSusChem, 2015, 8, 131-137.	3.6	63
43	Inorganic Gel-Derived Metallic Frameworks Enabling High-Performance Silicon Anodes. Nano Letters, 2019, 19, 6292-6298.	4.5	63
44	Designing activatable aptamer probes for simultaneous detection of multiple tumor-related proteins in living cancer cells. Biosensors and Bioelectronics, 2015, 68, 763-770.	5.3	61
45	Layer-stacked tin disulfide nanorods in silica nanoreactors with improved lithium storage capabilities. Nanoscale, 2012, 4, 4002.	2.8	60
46	Mesoporous carbon anchored with SnS2 nanosheets as an advanced anode for lithium-ion batteries. Electrochimica Acta, 2013, 111, 862-868.	2.6	58
47	G-quadruplex DNAzyme-based electrochemiluminescence biosensing strategy for VEGF165 detection: Combination of aptamer–target recognition and T7 exonuclease-assisted cycling signal amplification. Biosensors and Bioelectronics, 2015, 74, 98-103.	5.3	58
48	Inorganic Cyanogels and Their Derivatives for Electrochemical Energy Storage and Conversion. , 2019, 1, 158-170.		57
49	Insight into the effects of graphene oxide sheets on the conformation and activity of glucose oxidase: towards developing a nanomaterial-based protein conformation assay. Physical Chemistry Chemical Physics, 2012, 14, 9076.	1.3	52
50	Composition- and Aspect-Ratio-Dependent Electrocatalytic Performances of One-Dimensional Aligned Pt–Ni Nanostructures. Journal of Physical Chemistry C, 2013, 117, 19091-19100.	1.5	52
51	Highly loaded SnO 2 /mesoporous carbon nanohybrid with well-improved lithium storage capability. Journal of Power Sources, 2014, 247, 178-183.	4.0	52
52	Template-engaged synthesis of hollow porous platinum–palladium alloy nanospheres for efficient methanol electro-oxidation. Journal of Power Sources, 2016, 302, 195-201.	4.0	52
53	Synthesis of magnetic Fe ₃ O ₄ –Au hybrids for sensitive SERS detection of cancer cells at low abundance. Journal of Materials Chemistry B, 2015, 3, 4487-4495.	2.9	48
54	Controlled Self-Assembly of a Close-Packed Gold Octahedra Array for SERS Sensing Exosomal MicroRNAs. Analytical Chemistry, 2021, 93, 2519-2526.	3.2	48

#	Article	IF	CITATIONS
55	Multiplexed SERS Detection of Microcystins with Aptamer-Driven Core–Satellite Assemblies. ACS Applied Materials & Interfaces, 2021, 13, 6545-6556.	4.0	48
56	Designed synthesis of SnO ₂ @C yolk–shell spheres for high-performance lithium storage. CrystEngComm, 2014, 16, 517-521.	1.3	46
57	Mechanism of Methanol Decomposition on the Pt ₃ Ni(111) Surface: DFT Study. Journal of Physical Chemistry C, 2017, 121, 9348-9360.	1.5	46
58	Tubelike Gold Sphere–Attapulgite Nanocomposites with a High Photothermal Conversion Ability in the Near-Infrared Region for Enhanced Cancer Photothermal Therapy. ACS Applied Materials & Interfaces, 2016, 8, 10243-10252.	4.0	45
59	Immobilization and direct electrochemistry of cytochrome c at a single-walled carbon nanotube-modified electrode. Journal of Solid State Electrochemistry, 2006, 11, 390-397.	1.2	42
60	Assembling CoSn3 nanoparticles on multiwalled carbon nanotubes with enhanced lithium storage properties. Nanoscale, 2011, 3, 1798.	2.8	41
61	Pyrolysis of cyano-bridged hetero-metallic aerogels: a general route to immobilize Sn–M (M = Fe, Ni) alloys within a carbon matrix for stable and fast lithium storage. Nanoscale, 2018, 10, 4962-4968.	2.8	40
62	Vertically ordered Ni3Si2/Si nanorod arrays as anode materials for high-performance Li-ion batteries. Nanoscale, 2012, 4, 5343.	2.8	39
63	Graphene Quantum Dots Wrapped Gold Nanoparticles with Integrated Enhancement Mechanisms as Sensitive and Homogeneous Substrates for Surface-Enhanced Raman Spectroscopy. Analytical Chemistry, 2019, 91, 7295-7303.	3.2	39
64	Instability Induced by Ultraviolet Light in ZnO Thin-Film Transistors. IEEE Transactions on Electron Devices, 2014, 61, 1431-1435.	1.6	38
65	New Insights into the Effects of Thermal Treatment on the Catalytic Activity and Conformational Structure of Glucose Oxidase Studied by Electrochemistry, IR Spectroscopy, and Theoretical Calculation. Journal of Physical Chemistry B, 2010, 114, 12754-12764.	1.2	37
66	Highly Reversible and Fast Lithium Storage in Grapheneâ€Wrapped SiO ₂ Nanotube Network. ChemElectroChem, 2015, 2, 508-511.	1.7	37
67	Enhancing the Plasmon Resonance Absorption of Multibranched Gold Nanoparticles in the Near-Infrared Region for Photothermal Cancer Therapy: Theoretical Predictions and Experimental Verification. Chemistry of Materials, 2019, 31, 471-482.	3.2	36
68	General Layer-By-Layer Approach To Composite Nanotubes and Their Enhanced Lithium-Storage and Gas-Sensing Properties. Chemistry of Materials, 2009, 21, 5264-5271.	3.2	35
69	3D Graphene Hollow Nanospheres@Palladiumâ€Networks as an Efficient Electrocatalyst for Formic Acid Oxidation. Advanced Materials Interfaces, 2015, 2, 1500321.	1.9	35
70	Cyano-bridged coordination polymer hydrogel-derived Sn–Fe binary oxide nanohybrids with structural diversity: from 3D, 2D, to 2D/1D and enhanced lithium-storage performance. Nanoscale, 2016, 8, 9828-9836.	2.8	35
71	Carbon nanotubes supported cerium dioxide and platinum nanohybrids: Layer-by-layer synthesis and enhanced electrocatalytic activity for methanol oxidation. Journal of Power Sources, 2015, 287, 203-210.	4.0	34
72	Hybrid Organic–Inorganic Gel Electrocatalyst for Stable Acidic Water Oxidation. ACS Nano, 2019, 13, 14368-14376.	7.3	34

#	Article	IF	CITATIONS
73	A Versatile Approach for the Synthesis of ZnO Nanorod-Based Hybrid Nanomaterials via Layer-by-Layer Assembly. Journal of Physical Chemistry C, 2009, 113, 8147-8151.	1.5	33
74	Self-assembled graphene-wrapped SnO2 nanotubes nanohybrid as a high-performance anode material for lithium-ion batteries. Journal of Alloys and Compounds, 2015, 626, 234-238.	2.8	32
75	Highly sensitive methyltransferase activity assay and inhibitor screening based on fluorescence quenching of graphene oxide integrated with the site-specific cleavage of restriction endonuclease. Chemical Communications, 2014, 50, 10691-10694.	2.2	30
76	Rational synthesis of Ni nanoparticle-embedded porous graphitic carbon nanosheets with enhanced lithium storage properties. Nanoscale, 2015, 7, 18211-18217.	2.8	30
77	Enhanced cathode performances of amorphous FePO4 hollow nanospheres with tunable shell thickness in lithium ion batteries. Electrochemistry Communications, 2012, 18, 1-3.	2.3	29
78	Highly Selective Fluorescence Determination of the Hematin Level in Human Erythrocytes with No Need for Separation from Bulk Hemoglobin. Analytical Chemistry, 2016, 88, 3935-3944.	3.2	29
79	Boosting Long-Range Surface-Enhanced Raman Scattering on Plasmonic Nanohole Arrays for Ultrasensitive Detection of MiRNA. ACS Applied Materials & Interfaces, 2021, 13, 18301-18313.	4.0	29
80	Hydrogel-Derived Three-Dimensional Porous Si-CNT@G Nanocomposite with High-Performance Lithium Storage. Wuli Huaxue Xuebao/ Acta Physico - Chimica Sinica, 2020, 36, 1905034-0.	2.2	29
81	Taming the challenges of activity and selectivity in the electrochemical nitrogen reduction reaction using graphdiyne-supported double-atom catalysts. Journal of Materials Chemistry A, 2021, 9, 8489-8500.	5.2	28
82	Three-dimensional mesoporous Sn–Ni@C network derived from cyanogel coordination polymers: towards high-performance anodes for lithium storage. CrystEngComm, 2013, 15, 10340.	1.3	27
83	Chemically Binding Scaffolded Anodes with 3D Graphene Architectures Realizing Fast and Stable Lithium Storage. Research, 2019, 2019, 8393085.	2.8	26
84	A General Approach for Uniform Coating of a Metal Layer on MWCNTs via Layer-by-Layer Assembly. Journal of Physical Chemistry C, 2009, 113, 17387-17391.	1.5	24
85	Functionalization of ZnO nanorods with γ-Fe2O3 nanoparticles: Layer-by-layer synthesis, optical and magnetic properties. Materials Chemistry and Physics, 2010, 124, 908-911.	2.0	23
86	Leakage-free polypyrrole–Au nanostructures for combined Raman detection and photothermal cancer therapy. Journal of Materials Chemistry B, 2017, 5, 7949-7962.	2.9	23
87	Label-Free Raman Observation of TET1 Protein-Mediated Epigenetic Alterations in DNA. Analytical Chemistry, 2019, 91, 7304-7312.	3.2	23
88	Raman observation of a molecular signaling pathway of apoptotic cells induced by photothermal therapy. Chemical Science, 2019, 10, 10900-10910.	3.7	23
89	FePO4 nanoparticles embedded in a large mesoporous carbon matrix as a high-capacity and high-rate cathode for lithium-ion batteries. Electrochimica Acta, 2013, 92, 433-437.	2.6	22
90	Graphene-wrapped single-crystalline Fe ₃ O ₄ nanorods with superior lithium-storage capabilities. New Journal of Chemistry, 2014, 38, 4036.	1.4	22

#	Article	IF	CITATIONS
91	Hybrid aerogel-derived Sn–Ni alloy immobilized within porous carbon/graphene dual matrices for high-performance lithium storage. Journal of Colloid and Interface Science, 2017, 501, 267-272.	5.0	22
92	Confining ultrafine ZnSe nanoparticles in N,Se-codoped carbon matrix using a direct solid state reaction approach for boosting sodium storage performance. Journal of Alloys and Compounds, 2020, 840, 155703.	2.8	22
93	Facile preparation of CuO@SnO ₂ nanobelts as a high-capacity and long-life anode for lithium-ion batteries. RSC Advances, 2014, 4, 34417-34420.	1.7	21
94	Porous Si spheres encapsulated in carbon shells with enhanced anodic performance in lithium-ion batteries. Materials Research Bulletin, 2014, 55, 71-77.	2.7	21
95	The solid state electrochemistry of samarium (III) hexacyanoferrate (II). Journal of Solid State Electrochemistry, 2004, 8, 538.	1.2	20
96	Effects of guanidinium ions on the conformational structure of glucose oxidase studied by electrochemistry, spectroscopy, and theoretical calculations: towards developing a chemical-induced protein conformation assay. Physical Chemistry Chemical Physics, 2012, 14, 5824.	1.3	19
97	Facile synthesis of graphene supported FeSn2 nanocrystals with enhanced Li-storage capability. RSC Advances, 2014, 4, 17401.	1.7	19
98	Mechanistic Insight into the Facet-Dependent Adsorption of Methanol on a Pt ₃ Ni Nanocatalyst. Journal of Physical Chemistry C, 2015, 119, 18352-18363.	1.5	19
99	Hydrogel-Derived Nanoporous Sn–In–Ni Ternary Alloy Network for High-Performance Lithium-Storage. Electrochimica Acta, 2016, 210, 530-538.	2.6	19
100	Double-Network Gel-Enabled Uniform Incorporation of Metallic Matrices with Silicon Anodes Realizing Enhanced Lithium Storage. ACS Applied Energy Materials, 2019, 2, 2268-2275.	2.5	19
101	Nitrogen-Doped Graphdiyne Quantum Dots for Electrochemical Chloramphenicol Quantification in Water. ACS Applied Nano Materials, 2021, 4, 12755-12765.	2.4	19
102	Confining SnSe nanobelts in 3D rGO aerogel for achieving stable and fast lithium storage. Materials Research Bulletin, 2019, 115, 80-87.	2.7	18
103	The Solid State Electrochemistry of Dysprosium(III) Hexacyanoferrate(II). Electroanalysis, 2005, 17, 1583-1588.	1.5	17
104	DNA strand-displacement-induced fluorescence enhancement for highly sensitive and selective assay of multiple microRNA in cancer cells. Chemical Communications, 2014, 50, 1012-1014.	2.2	17
105	Plasmonic SERS Biosensor Based on Multibranched Gold Nanoparticles Embedded in Polydimethylsiloxane for Quantification of Hematin in Human Erythrocytes. Analytical Chemistry, 2021, 93, 1025-1032.	3.2	17
106	Facile and efficient room temperature solid state reaction enabled synthesis of antimony nanoparticles embedded within reduced graphene oxide for enhanced sodium-ion storage. Applied Surface Science, 2018, 444, 448-456.	3.1	15
107	Coral-shaped Au nanostructures for selective apoptosis induction during photothermal therapy. Journal of Materials Chemistry B, 2019, 7, 6224-6231.	2.9	15
108	Sensitivity-Improved SERS Detection of Methyltransferase Assisted by Plasmonically Engineered Nanoholes Array and Hybridization Chain Reaction. ACS Sensors, 2020, 5, 3639-3648.	4.0	15

#	Article	IF	CITATIONS
109	Electrochemical approach for the specific detection of hepatitis C virus based on site-specific DNA cleavage of BamHI endonuclease. Analytical Methods, 2010, 2, 135-142.	1.3	14
110	Electrochemical probing of the solution pH-induced structural alterations around the heme group in myoglobin. Physical Chemistry Chemical Physics, 2013, 15, 16941.	1.3	14
111	Probing the anticancer-drug-binding-induced microenvironment alterations in subdomain IIA of human serum albumin. Journal of Colloid and Interface Science, 2015, 445, 102-111.	5.0	14
112	Cyano-bridged coordination polymer gel as a precursor to a nanoporous In2O3–Co3O4 hybrid network for high-capacity and cycle-stable lithium storage. New Journal of Chemistry, 2015, 39, 8249-8253.	1.4	14
113	A Tumor Microenvironment-Triggered and Photothermal-Enhanced Nanocatalysis Multimodal Therapy Platform for Precise Cancer Therapy. Chemistry of Materials, 2021, 33, 9334-9347.	3.2	14
114	Electrochemical preparation and characterization of dysprosium hexacyanoferrate modified electrode. Journal of Solid State Electrochemistry, 2006, 10, 270-276.	1.2	13
115	Hollow porous SiO ₂ nanobelts containing sulfur for long-life lithium–sulfur batteries. RSC Advances, 2016, 6, 91179-91184.	1.7	12
116	Interpenetrating gels as conducting/adhering matrices enabling high-performance silicon anodes. Journal of Materials Chemistry A, 2021, 9, 12003-12008.	5.2	12
117	Solvothermal synthesis of carbon-coated tin nanorods for superior reversible lithium ion storage. Materials Research Bulletin, 2011, 46, 2278-2282.	2.7	11
118	Fluorescence quenching of graphene oxide combined with the site-specific cleavage of restriction endonuclease for deoxyribonucleic acid demethylase activity assay. Analytica Chimica Acta, 2015, 869, 74-80.	2.6	11
119	Stable and fast Siâ^Mâ^C ternary anodes enabled by interfacial engineering. Journal of Power Sources, 2022, 530, 231290.	4.0	11
120	Designed synthesis of NiO@polypyrrole hollow spheres for long-life lithium storage. lonics, 2015, 21, 359-364.	1.2	10
121	Facile template-directed synthesis of carbon-coated SnO2 nanotubes with enhanced Li-storage capabilities. Materials Chemistry and Physics, 2015, 163, 581-586.	2.0	10
122	Hermetically Coated and Wellâ€Separated Co ₃ O ₄ Nanophase within Porous Graphitic Carbon Nanosheets: Synthesis, Confinement Effect, and Improved Lithiumâ€Storage Capacity and Durability. Chemistry - A European Journal, 2016, 22, 9599-9606.	1.7	10
123	Facile fabrication of sheet-on-sheet hierarchical nanostructured Sb/C composite with boosting sodium storage. Journal of Colloid and Interface Science, 2019, 545, 200-208.	5.0	10
124	Gelâ€Derived Amorphous Bismuth–Nickel Alloy Promotes Electrocatalytic Nitrogen Fixation via Optimizing Nitrogen Adsorption and Activation. Angewandte Chemie, 2021, 133, 4321-4327.	1.6	10
125	Large-scale synthesis of water-soluble nanowires as versatile templates for nanotubes. Chemical Communications, 2011, 47, 1006-1008.	2.2	9
126	Cyanogel-derived nanoporous Sn–Fe–Ni ternary oxide network for high-capacity and long-life lithium storage. Journal of Alloys and Compounds, 2017, 691, 250-254.	2.8	9

#	Article	IF	CITATIONS
127	Highly dispersed ultrafine palladium nanoparticles on three-dimensional mesoporous carbon for for formic acid electro-oxidation. Ionics, 2015, 21, 2609-2614.	1.2	8
128	Exploring the methanol decomposition mechanism on the Pt ₃ Ni(100) surface: a periodic density functional theory study. Physical Chemistry Chemical Physics, 2018, 20, 10132-10141.	1.3	8
129	Hybrid-Cyanogels Induced Sandwich-like N,P-Carbon/SnNi10P3 for Excellent Lithium Storage. ACS Applied Energy Materials, 2019, 2, 3683-3691.	2.5	8
130	New insights into the structure-property relation in ZnCo2O4 nanowire and nanosheet arrays. Journal of Alloys and Compounds, 2020, 817, 152692.	2.8	8
131	Covalent binding of holey Si–SiC layer on graphene aerogel with enhanced lithium storage kinetics and capability. Surface and Coatings Technology, 2021, 420, 127336.	2.2	8
132	A bioinspired hollow g-C ₃ N ₄ –CuPc heterostructure with remarkable SERS enhancement and photosynthesis-mimicking properties for theranostic applications. Chemical Science, 2022, 13, 6573-6582.	3.7	8
133	Ceneral Self-Assembly Route toward Sparsely Studded Noble-Metal Nanocrystals inside Graphene Hollow Sphere Network for Ultrastable Electrocatalyst Utilization. ACS Applied Materials & Interfaces, 2015, 7, 20061-20067.	4.0	7
134	Polypyrrole-derived nitrogen-doped carbon nanotubes: Template-directed synthesis and enhanced sodium-storage performance. Journal of the Taiwan Institute of Chemical Engineers, 2016, 65, 552-557.	2.7	7
135	Fluorescence activation imaging of localization, distribution, and level of miRNA in various organelles inside cells. Talanta, 2018, 186, 406-412.	2.9	7
136	Cascade signal amplification sensing strategy for highly specific and sensitive detection of homologous microRNAs in different molecular subtypes of breast cancer. Analytica Chimica Acta, 2020, 1093, 86-92.	2.6	7
137	Rapid functionalization of carbon nanotube and its electrocatalysis. Frontiers of Chemistry in China: Selected Publications From Chinese Universities, 2007, 2, 369-377.	0.4	6
138	Tuning the electron transport band gap of bovine serum albumin by doping with Vb12. Chemical Communications, 2019, 55, 2853-2856.	2.2	6
139	Highly Biocompatible Plasmonically Encoded Raman Scattering Nanoparticles Aid Ultrabright and Accurate Bioimaging. ACS Applied Materials & amp; Interfaces, 2021, 13, 135-147.	4.0	6
140	Large-scale synthesis of water-soluble Na2SiF6 nanotubes with polyacrylic acid as a surfactant. Materials Research Bulletin, 2012, 47, 3923-3926.	2.7	5
141	Facile solid-state synthesis of Ni@C nanosheet-assembled hierarchical network for high-performance lithium storage. Journal of Power Sources, 2017, 358, 69-75.	4.0	5
142	Sn4P3-inlaid graphene oxide nanohybrid through low-temperature solid state reactions toward high-performance anode for sodium-ion batteries. Journal of the Taiwan Institute of Chemical Engineers, 2021, , .	2.7	5
143	Multiwalled carbon nanotubes anchored with maghemite nanocrystals for high-performance lithium storage. Materials Research Bulletin, 2015, 64, 106-111.	2.7	4
144	Facile hydrogel-derived sub-10Ânm tin–iron alloy embedded in 3D carbon nanocorals with improved cycle life and rate capability. Ionics, 2019, 25, 5287-5295.	1.2	2

#	Article	IF	CITATIONS
145	Chemical binding and conformal coating of sub-10Ânm Sn–Ni alloy layer on nanostructured carbon matrices enabling enhanced lithium storage. Surface and Coatings Technology, 2020, 400, 126068.	2.2	2
146	One-pot Synthesis of Sn/Mesoporous Carbon Composite in a Polyol System with Well-improved Lithium Storage Capability. Acta Chimica Sinica, 2015, 73, 151.	0.5	2
147	Modulating the electron transport energy levels of protein by doping with foreign molecule. Journal of Electroanalytical Chemistry, 2019, 851, 113472.	1.9	1